RSC Advances

PAPER

View Article Online
View Journal | View Issue

Cite this: *RSC Adv.*, 2021, **11**, 33036

An ink-jet printed dual-CD ratiometric fluorescent paper-based sensor for the visual detection of Cu^{2+}

Ying Li,[a] Fei Lu,[a] Qing-zhi Li,[a] Yi-hua Zhou, *[a] Jun Qian, *[a] Sheng Cao[b] and Chen-yu Wang[a]

Copper ion (Cu^{2+}) plays an important role in the human body because it is beneficial for metabolism. However, an excessive or slight amount of Cu^{2+} can cause various symptoms. Therefore, it is necessary for human health to realize the trace and visual detection of Cu^{2+}. Referring to traditional fluorescence test papers, the qualitative and semi-quantitative detection of Cu^{2+} could be realized by a dual-carbon dots (CDs) ratiometric fluorescent paper-based sensor with the advantages of environmental protection, portability and low cost. In this paper, the inkjet-printed test paper with the best mixing ratio of the two CDs has been researched to maximize the spectral energy transfer of ion detection (maximum color gamut expansion). Among them, the preparation method of b-CDs has been improved, increasing the photoluminescence quantum yield (PLQY) to 88.9%. The sensitivity detection limit of the double emission ratio sensor was 0.15 nM in solution, and the human eye can distinguish at least 3 μmol L^{-1} Cu^{2+} in the paper-based sensor. Compared with the traditional single-emission sensor, the human eye was more sensitive to the color change of the emission ratio sensor. The results indicate that we not only realized the micro detection of Cu^{2+} with convenient methods, but also provided a promising strategy for the visual detection of Cu^{2+}.

Received 21st July 2021
Accepted 23rd September 2021

DOI: 10.1039/d1ra05592e

rsc.li/rsc-advances

1. Introduction

Copper ion (Cu^{2+}) plays an essential role in the metabolism of the human body.[1] However, excessive Cu^{2+} intake may not only lead to various symptoms but also cause some neurological diseases, including Alzheimer's disease and Parkinson's disease.[2] Simultaneously, as heavy metal pollution in the living environment has increased in recent years, people must be vigilant about this metal ion in the surrounding environment. Therefore, it is very important to explore a probe that can detect the dose of Cu^{2+} in domestic water with high selectivity and accuracy.

Fluorescence analysis is a method of qualitative or quantitative analysis of a target based on the change of a fluorescent signal; it has high analytical sensitivity and strong selectivity, and it has been applied to medical diagnostics,[3] environmental monitoring,[4] explosives detection,[5] and food safety testing.[6] Although fluorescent sensors can be explored without complicated sample pretreatments, large equipment, and well-trained technicians, the qualitative and quantitative assays on a target species still have to rely on the aid of a fine fluorescence spectrometer. To achieve the aim of the observation of qualitative and semiquantitative assays by the naked eye, the fluorescent probes must be highly sensitive to the remarkable variations in the spectrum, including color and brightness.[7] Carbon dots (CDs) are fluorescent carbon nanometer materials under 10 nm in size; they were first discovered in 2004 during the purification of single-walled carbon nanotubes by electrophoresis.[8] CDs have many advantages, such as good photostability, tunable emissive color, good solubility in water and good biological compatibility, which are very suitable for the requirements of fluorescent sensors. However, the preparation of b-CDs and the improvement of photoluminous quantum yield (PLQY) are problems to be overcome in the current related research.

Inkjet printing transfers tiny droplets (picoliters, 10^{-9} mL) of the printing material to the designated area by a non-contact method. With the development of inkjet printing technology, inkjet inks have expanded from traditional dyes and pigments to various functional materials. At present, inkjet printing has been applied in chemistry,[9] biology,[10] life sciences[11] and printed electronics,[12] and it is widely used in other fields. Because the fluorescence response of a single CD to copper ions is not obvious enough, we preferred the ratio fluorescence analysis method to construct the detection test paper. Ratiometric fluorescent analysis is a new detection method to determine the concentration of an analyte by measuring the fluorescence intensity at two (or more) different wavelengths under the same excitation wavelength and using the ratio as a characterization parameter. Ratiometric fluorescent paper-based sensors have

[a]*School of Printing and Packaging, Wuhan University, Wuhan 430079, Hubei, China. E-mail: yihuazhou@whu.edu.cn; qianjungreat@whu.edu.cn; Tel: +86 13317169910; +86 18971135061*

[b]*Wuhan Donghu University, Wuhan 430079, Hubei, China*

attracted considerable attention as useful analytical instruments due to their visual detection, low cost, portability and easy operation. To construct a ratiometric fluorescent sensor that involves two or more fluorescence materials working together, the optimization of the ratio of the involved fluorescence materials is a key step. This ratio determination can be carried out by standard assays in solution, which is straightforward but time-consuming. Ink-jet printing can precisely control the proportions and patterns of multiple components, which can help to properly design and adjust the ratio of the fluorescence intensity of the sensor. In addition, the choice of carrier is very important for the sensitivity of ion detection. Some researchers usually choose filter paper as the carrier.[7] However, filter paper cannot be used for accurate semi-quantitative testing because of its blue fluorescence.

Herein, red CDs (r-CDs) and blue CDs (b-CDs) were used to construct a ratio-type fluorescence sensor, which was used to realize a test paper with color visualization caused by the change of Cu^{2+}. Among the two fluorescent groups, b-CDs were used as internal standard probes to enhance visual contrast, and r-CDs were used as sensing probes to achieve a linear fluorescence intensity change. Citric acid and ethylenediamine were used as precursors for preparing the b-CDs, and they were dispersed in ethanol. The PLQY of the b-CDs was increased to 88.9%. At the same time, to satisfy the high selectivity and high precision of Cu^{2+} sensing in the dual emission ratiometric fluorescent sensor, we present a simple, fast and precise method to construct fluorescent sensors with optimized ratios by ink-jet printing. Bond paper was used as the carrier of the CDs, which improved the visual inspection effect of the test paper. The preset color model processed by the printer created significant amounts of ratiometric fluorescent sensors with different ratios in a single run. We found that when the density ratio of the r-CDs/b-CDs probe was 10 : 3, the paper-based sensor had the largest color gamut. When the concentration of Cu^{2+} was added from 3 to 18 μmol L^{-1}, the fluorescence intensity ratio showed a good linear relationship from 525 to 675 nm, and the detection limit reached 0.15 nM, which was lower than the maximum level of copper in drinking water (20 μmol L^{-1}).

2. Experimental

2.1 Reagents and instruments

ρ-Phenylenediamine (ρ-PDA), petroleum ether (PE), silica gel ($xSiO_2 \cdot yH_2O$), ethyl acetate (EA), citric acid (CA), ethylenediamine (EDA), disodium hydrogen phosphate ($Na_2HPO_4 \cdot 12H_2O$), sodium dihydrogen phosphate ($NaH_2PO_4 \cdot 2H_2O$), sodium chloride (NaCl), potassium chloride (KCl), ethanol, quartz sand, deionized water, and securities paper were purchased from Aladdin Ltd. All chemicals were used as received and did not require further purification. Deionized water (18.2 MΩ cm) was produced by a Millipore water purification system.

A DZF-6020 vacuum dryer (Shanghai Xinmiao Co., Ltd.), AL-204-IC electronic analysis balance (METTLER-TOLEDO), HP Printer 2050 (China Hewlett–Packard Co., Ltd.), KQ-300DE ultrasound cleaner (Kunshan Instrument Co., Ltd.), H1650-W centrifuge (Hunan Instrument Co., Ltd.), FP-6500 fluorescence spectrometer (Jusco (Shanghai) Trading Co., Ltd), UV-3600 ultraviolet-visible spectrometer (Shimadzu Instruments and Equipment Co., Ltd.), TEM-2100 transmission electron microscope (Japan Electronics Co., Ltd.), FT-IR-5700 (Thermo Co., USA), X-ray photoelectron spectroscope (Thermo Fisher, UK), H-G lamp, Canon EOS 350D digital camera, and USB portable UV lamp (365 nm) were used.

2.2 Synthesis of r-CDs

According to the reported solvothermal method, r-CDs were prepared and slightly modified.[13] ρ-PDA (0.5 g) was dissolved in 50 mL ethanol, and the solution was transferred to a polytetrafluoroethylene reactor. Then, it was heated in a vacuum drying chamber at 200 °C for 12 hours and cooled naturally to room temperature. The mixture was purified on a silica gel column and dried in a rotary evaporator using ethyl acetate as the eluent. The final product was obtained and the purified r-CDs were dispersed in 50 mL ethanol for further use.

2.3 Synthesis of b-CDs

0.21 g (1 mmol) CA and 0.18 g (3 mmol) EDA were dissolved in 5 mL deionized water by magnetic stirring to obtain a clarified transparent solution.[14] The solution was transferred to a 20 mL reactor and placed in an oven to heat to 160 °C for 4 h. The product was washed with a large amount of ethanol and centrifuged at 5000 rpm for 5 min. b-CDs were prepared by freeze-drying 24 hours after separation and purification, and the solid was ground into powder for use.

2.4 Detection of Cu^{2+} by the ratiometric sensor

The double emission rate fluorescent probe was prepared by mixing r-CDs and b-CDs. They were mixed in 2 mL PBS buffer with different proportions and compared with each other. Because pH can affect the fluorescence performance of CDs, the pH of the solution was controlled at 7.4.[15] Different concentrations of copper ions were added to the solution of a specific fluorescence probe, and the fluorescence spectrum was recorded by a fluorescence spectrometer after reaction for 3 minutes.

2.5 Selectivity and interference tests

For the selectivity study of metal ions, other metal ions (including Ag^+, Co^{2+}, Ba^{2+}, Al^{3+}, Mn^{2+}, Fe^{2+}, K^+, Na^+, Zn^{2+}, Ni^+, and Cu^{2+}) were added to 1 mL PBS buffer solution (with the fluorescence probe, pH 7.4). The final concentration was 10 μmol L^{-1}, respectively.

To observe the interference of the fluorescence probe with Cu^{2+}, the metal ions (20 μmol L^{-1}) above (1 mL) were added to 1 mL PBS buffer solution (pH 7.4) to achieve the final concentration (10 μmol L^{-1}). Then, 1 mL Cu^{2+} (in PBS buffer solution) with a concentration of 10 μmol L^{-1} was added to the mixture, and the fluorescence spectrum was recorded again to detect the anti-interference ability of the probe.

2.6 Fabrication of paper-based sensors by ink-jet printing

In this study, a thermal ink-jet printer (HP 8020) was applied to print the CDs and metal ions. In general, the surface tension of the ink controlled the generation of tiny droplets (typically around several to tens of picoliters) and determined the spreading behavior of the ink on the substrate as well. The viscosity of the ink strongly affected the pinch-off of the droplet at the nozzle and the permeation of ink on the printing substrate. First, we developed two formulations of the CD inks (2 mg mL^{-1} of r-CDs, 10 mM PBS buffer solution, pH 7.4; 2 mg mL^{-1} of b-CDs, 10 mmol L^{-1} PBS buffer solution, pH 7.4) to obtain an appropriate surface tension and viscosity (in the range of 40 × 10^{-3} N m^{-1} and 4 mPa).[16] The ink solutions retained their original properties after 24 h at room temperature.

The ink cartridge was cleaned with deionized water until the ink residue was completely removed. The cartridge was dried in an oven at 60 °C for 3 hours and then taken out. The R-CDs and b-CDs fluorescent inks were injected into magenta (M) and cyan (C) ink cartridges, respectively. The red and blue color blocks with a density of 10 : 1–10 : 10 were stacked respectively on the securities paper. The ink was printed on the stock paper by an ink-jet printer connected to a computer; the printing times were repeated 10 times (300 dpi was used). Finally, the stock paper showed strong color fluorescence under UV light of 365 nm.

To prove the selective response of the paper-based sensor, we directly ink-jet printed the ten metal ion solutions described in Section 2.5 on the prepared paper-based sensor, and we observed the fluorescence changes of the sensor's response to the ions.

Anti-interference of test paper detection: 0.1 mL of 10 μmol L^{-1} of the other ten metal ions were mixed, and then 1 mL Cu^{2+} (in PBS buffer solution) with different concentrations (0 μmol L^{-1}, 6 μmol L^{-1}, 12 μmol L^{-1}, 18 μmol L^{-1}) was added. The mixed solutions of the four concentrations were printed on the test paper, respectively, and the color changes were observed.

3. Results and conclusion

3.1 Characterization and optical properties of r-CDs/b-CDs

The properties of the r-CDs were characterized by transmission electron microscopy (TEM), UV-visible spectrophotometry (UV-Vis) and fluorescence spectroscopy (FL). As shown in Fig. 1a,

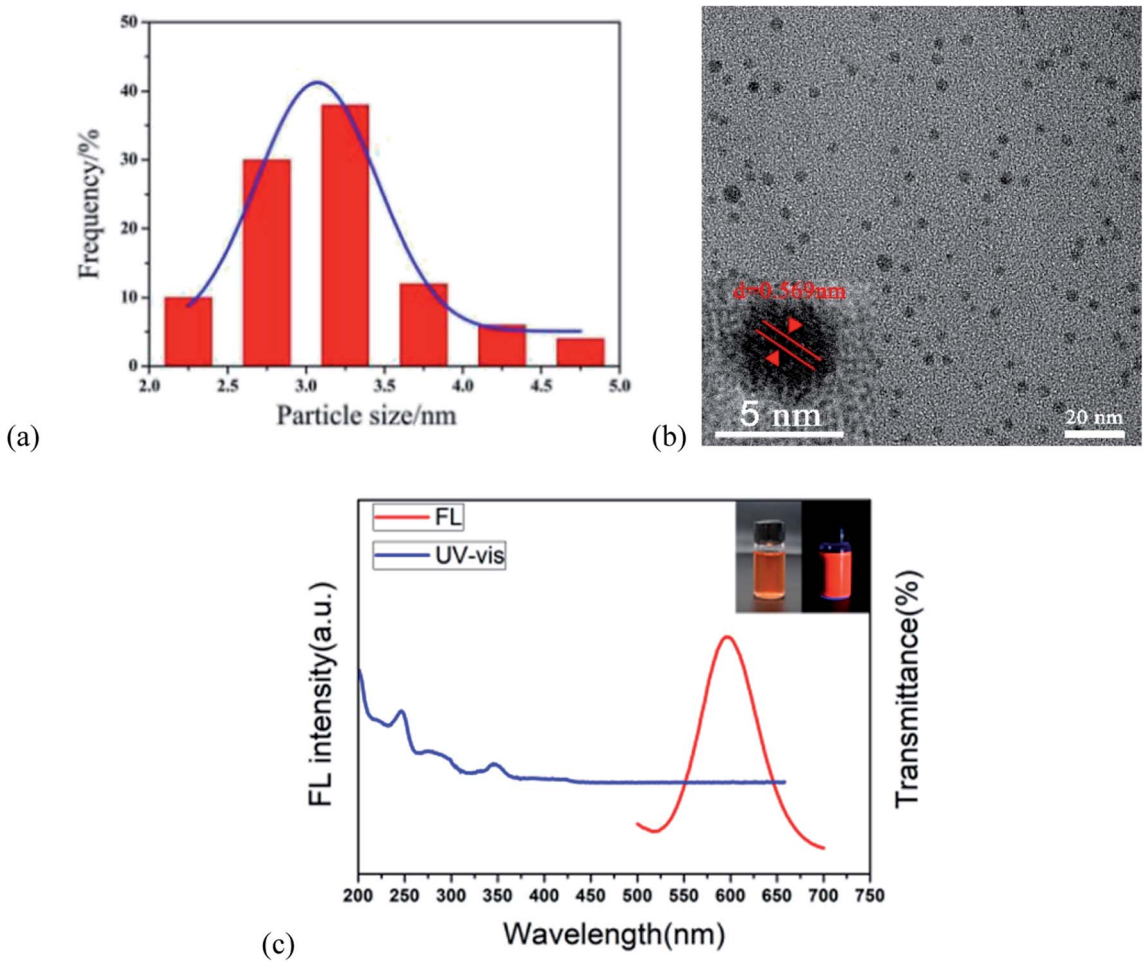

Fig. 1 Characteristics and optical properties of the r-CDs. (a) The size distribution of the r-CDs; (b) TEM image of the r-CDs (illustration shows the HRTEM of the r-CPDs); (c) UV and FL spectra of the r-CDs (the illustration shows the corresponding colors under daylight and a 365 nm UV lamp).

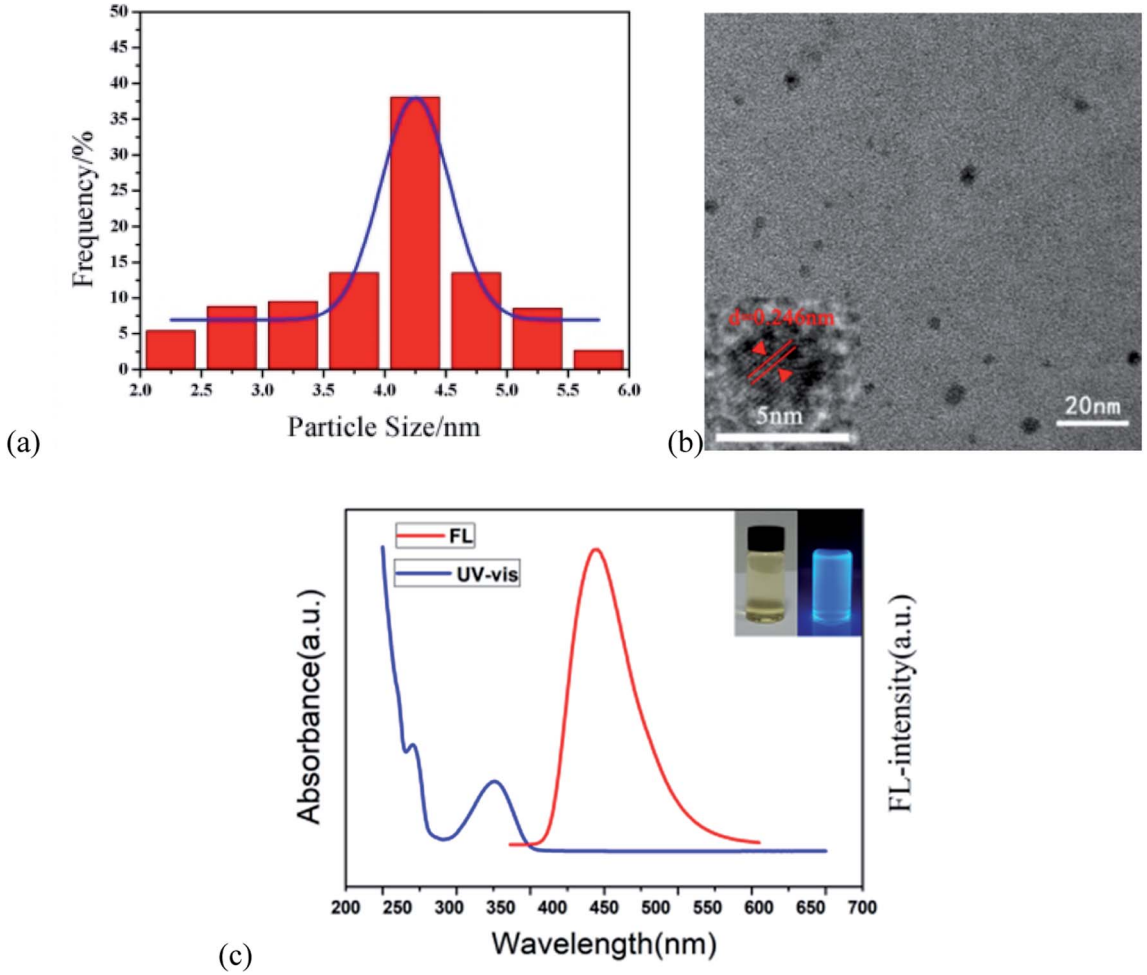

Fig. 2 Characteristics and optical properties of b-CDs. (a) The size distribution of the b-CDs; (b) the TEM image of the b-CDs (inset shows the HRTEM image of the b-CPDs); (c) the UV and FL spectra of the b-CDs (inset shows the corresponding colors under daylight and a 365 nm UV lamp).

the maximum particle size of the r-CDs reached 8.13 nm and the average particle size was 2.96 nm, with good monodispersity in ethanol and water. The crystal grains were uniformly dispersed in the solvent, and clear lattice fringes could be observed (0.569 nm, as shown in Fig. 1b). The FL spectra of the r-CDs showed an emission peak at 600 nm which was excited by 360 nm UV light (the red curve in Fig. 1c). The UV-vis spectra showed two characteristic absorption peaks centered at 246 and 345 nm, as well as the shoulder of the absorption curve at 276 nm (blue curve in Fig. 1c). These two peaks belonged to the π–π* transition of C=C and C=N in the aromatic rings, which was the same as that of ρ-PDA.[17–19] The weak band at 276 nm was attributed to the transition of the unshared electrons from the π–π conjugation of $-NH_2$ and benzene rings.[20] Light pink was observed in daylight, while bright orange-red fluorescence was observed in a 365 nm UV lamp (inset in Fig. 1c).

The b-CDs were prepared by the bottom-up hydrothermal method. Fig. 2a shows the good monodispersity of b-CDs in ethanol and water with an average particle size of 4.05 nm. It can be seen that the b-CDs were spherical in shape and dispersed uniformly in an aqueous solution without agglomeration (Fig. 2b). The lattice spacing of 0.246 nm indicated that the b-CDs had a graphite-like structure, as shown in the inset of Fig. 2a. The FL spectrum of the b-CDs showed blue emission centered at 443 nm with an excitation of 360 nm (the red line in Fig. 2c), and the PLQY was 88.9%. They were almost colorless and transparent under daylight and showed bright blue fluorescence under a 365 nm UV lamp (inset in Fig. 2c). The UV-vis spectra showed two characteristic absorption peaks at 260 and 352 nm (the blue curve in Fig. 2c); the absorption peaks at 260 nm were mainly due to the π–π* transition of the C=C double bond, and the absorption peaks at 352 nm were due to the transition of n–π* of the C=O double bond.

In addition, FTIR and XPS were used to study the possible chemical bonds and functional groups in the r-CDs. The FTIR spectrum in Fig. 3a shows a band at 3406 cm^{-1}, which could be classified as the N–H stretching vibration. The other three peaks at 1625, 1515 and 1307 cm^{-1} are the C=N, C=C and C–N= tensile vibrations, respectively. The peak value at 829 cm^{-1} corresponds to the outer plane bending of the benzene ring.[21–23]

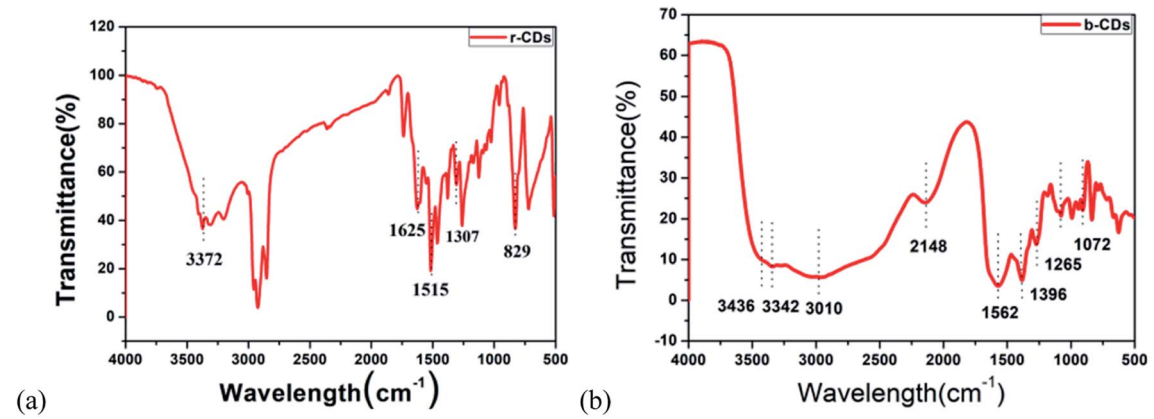

Fig. 3 (a) FT-IR image of the r-CDs. (b) FT-IR image of the b-CDs.

Furthermore, the deconvolution peaks at 398.6, 399.3 and 400 eV of the N1s band are associated with pyridine N, amino N and pyrrole N, respectively,[24,25] as shown in Fig. 4a–c. Together with the UV-vis spectra, these measurements confirmed that incomplete carbonization resulted in a large number of ρ-PDA ligands remaining on the surface of the r-CDs.

As shown in Fig. 3b, the peak at 3436 cm^{-1} could be seen as the stretching vibration of the –C–H bond, which indicated that the b-CDs contained saturated alkyl groups. Moreover, the peak at 3342 cm^{-1} could be seen as the stretching vibration of the –OH bond. The strong peak at 3010 cm^{-1} could be seen as the vibration of the $–NH_2$ bond. At the same time, the stretching vibration of the –C=O–NH (peptide) bond could be deduced at 1562 cm^{-1}, and the stretching vibration of the –C–O bond could be deduced at 1396/1072 cm^{-1}.[26] The peak at 1265 cm^{-1} was due to the stretching vibration of the C–O bond.[27] Compared with the characteristic peak position of the standard infrared spectrum, the characteristic peaks of the N–H bond and the C=O bond in the FT-IR spectrum belonged to the characteristic peak of the amide bond, which indicated that the b-CDs prepared in the research contain amide bonds.[28] Fig. 4d, e and f show that the peaks at 284.6, 285.3, 286.28 and 288 eV (deconvolution of the C 1s bands of b-CDs) are associated with the bonds of –C–/–C=C–, –C–O–, –N–C=N–, and –O–C=O–, respectively.

To explore the mechanism of Cu^{2+}-induced fluorescence, the response of the r-CDs and b-CDs to Cu^{2+} was researched. Fig. 5a and b show the fluorescence intensity changes of the b-CDs and r-CDs in the presence of Cu^{2+} within 2 hours, respectively. The relative standard deviations of the linear fitting curves in Fig. 5a and b were 0.036 and 0.005, indicating the good optical stability of the two CDs. When Cu^{2+} was added to a mixture of b-CDs and r-CDs, the particle sizes of the r-CDs/b-CDs increased significantly. The average particle sizes of the r-CDs and b-CDs were 2.96 nm and 4.05 nm, respectively, while the particle size increased to 13.01 nm after adding Cu^{2+} (Fig. 5c and d). According to our conclusion, the increase in the ion size of the r-CDs/b-CDs was due to the coordination of Cu^{2+}. The smaller r-CDs adsorbed on the surfaces of the larger b-CDs through the Cu^{2+}, and the larger π-PDA ligand conjugation system led to the transfer of a π electron into the vacant d orbital of Cu^{2+}.[29,30] As shown in the UV-Vis spectrum in Fig. 5e, a new absorption band of 400–600 nm appeared in the r-CDs solution with increasing concentration of Cu^{2+}. On the other hand, the UV-Vis spectrum of the b-CDs remained unchanged after Cu^{2+} was added. These results confirmed that when Cu^{2+} was added to the ratio probe, the charge was transferred from the ρ-PDA ligand to the surface of the r-CDs, resulting in the fluorescence quenching of the r-CDs.[31–35]

According to the principle of ligand metal charge transfer (LMCT) shown in Fig. 6a, the competitive binding of r-CDs and Cu^{2+} ions in solution led to aggregation of the r-CDs. The fluorescence spectra of b-CDs and r-CDs showed the maximum emissions at 443 and 600 nm, respectively (at the excitation wavelength of 360 nm). The fluorescence intensity ratio of r-CDs/b-CDs was changed for further study. It was found that the color gamut evolution of the double emission ratio probe was maximized only when the ratio was 4 : 1. In this case, the corresponding coordinates of the b-CDs and r-CDs were (0.15, 0.13) and (0.65, 0.3), respectively. The chromaticity coordinates of the r-CDs/b-CDs would change along the line between the two kinds of carbon dots in the chromaticity coordinate system, which was the basis of visual detection. Both nanoparticles could be excited at the same time, and double emission peaks were observed at 443 and 600 nm. At the same time, Fig. 6b shows the corresponding fluorescence color under a 365 nm UV lamp. Compared with b-CDs and r-CDs, the ratio sensor showed orange-red fluorescence, which indicated remarkable variations in the spectrum, including color and brightness. Moreover, the fluorescence intensity at 600 nm (F) in Fig. 6c decreased proportionately ranging from 3 to 18 μmol L^{-1} Cu^{2+} ions with good linearity, based on the correlation coefficient (R^2) of 0.99918 (in Fig. 6d). The detection limit was 3 times the background standard deviation divided by the linear slope ($3S/k$), which was calculated as 0.15 nM.

Moreover, the photobleaching tolerance of the ratio sensor was characterized by continuous irradiation of the H-G lamp with a 365 nm wavelength. As shown in Fig. 7, the ratio of the

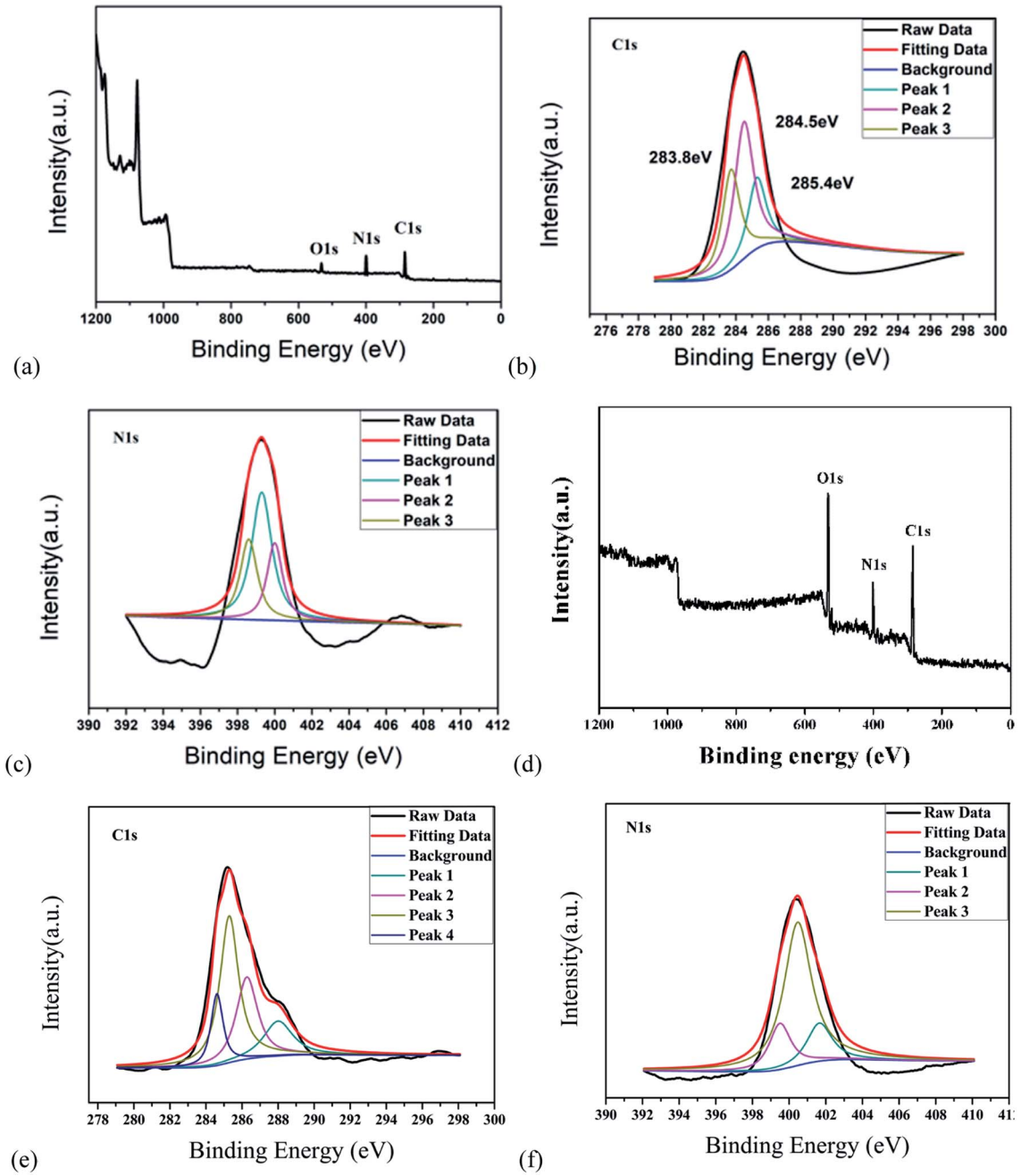

Fig. 4 (a) General XPS diagram of the r-CDs. (b) XPS diagram of C1s of the r-CDs. (c) XPS diagram of N1s of the r-CDs. (d) The general XPS diagram of the b-CDs. (e) XPS diagram of C1s of the b-CDs. (f) XPS diagram of N1s of the b-CDs.

fluorescence intensity at 600 and 443 nm showed almost no change within 1 hour, and the relative standard deviation of the linear fitting curve was 0.063, indicating relatively high fluorescence stability.

3.2 Detection of Cu^{2+} with the R-CDs/R-CDs sensor

In order to evaluate the sensitivity of the r-CDs/b-CDs sensor to Cu^{2+}, the fluorescence response of r-CDs/b-CDs solution (10 μmol L^{-1}, pH 7.4) to Cu^{2+} with different concentrations from 0 to 50 μmol L^{-1} was measured.

As shown in Fig. 8a and b, two distinct peaks at 600 nm and 443 nm can be recorded under a single excitation. The fluorescence intensity of the r-CDs decreased significantly with the addition of Cu^{2+}, while the b-CDs were not affected. As shown in Fig. 8c, when the Cu^{2+} concentration changed from 3 to 18 μmol L^{-1}, the ratio of the fluorescence intensity to the original fluorescence intensity (F/F_0, $F_0 = 2400$) of the sensor at 600 nm had a good linear relationship with the concentration of Cu^{2+}. The linear equation was $(F/F_0) = 0.4883–0.025\ Cu^{2+}$ (the correlation coefficient $R^2 = 0.99918$). As shown in Fig. 8c, the detection limit was calculated to be not much different from that in Fig. 6.

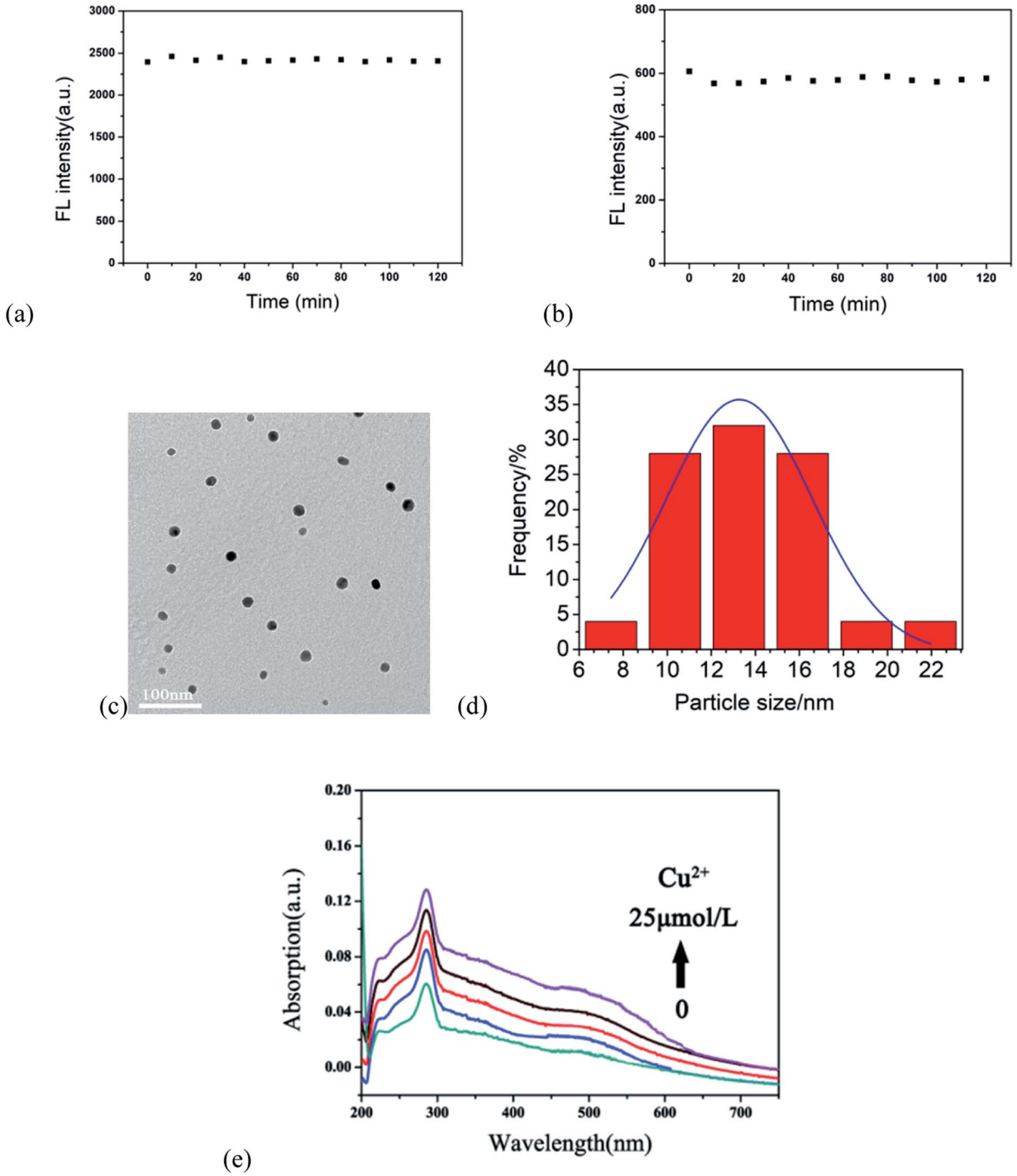

Fig. 5 The effect of 18 μmol L^{-1} Cu^{2+} on the fluorescence of (a) b-CDs and (b) r-CDs in 2 h; (c) TEM image of the small r-CDs adsorbed onto the larger b-CDs after the addition of Cu^{2+} ions; (d) particle sizes of r-CDs/b-CDs + Cu^{2+}; (e) evolution of the UV-vis spectrum of r-CDs after the addition of Cu^{2+}.

This test result was in full compliance with the EPA regulation that the maximum allowable content of Cu^{2+} in drinking water is 20 μM. This work showed that the r-CDs alone used to detect Cu^{2+} had no obvious fluorescence color change, so that it could not be distinguished by the naked eye, especially for low Cu^{2+} with a concentration range of 3 to 18 μmol L^{-1}.

3.3 Optimizing experimental conditions for detecting Cu^{2+} with the ratio fluorescence paper-based sensor

According to the above strategy, we prepared a fluorescent test paper for visual semi-quantitative detection of Cu^{2+} ions. However, when the dual-colored carbon dots with a fluorescence intensity ratio of 4 : 1 (r-CDs/b-CDs) were transferred to

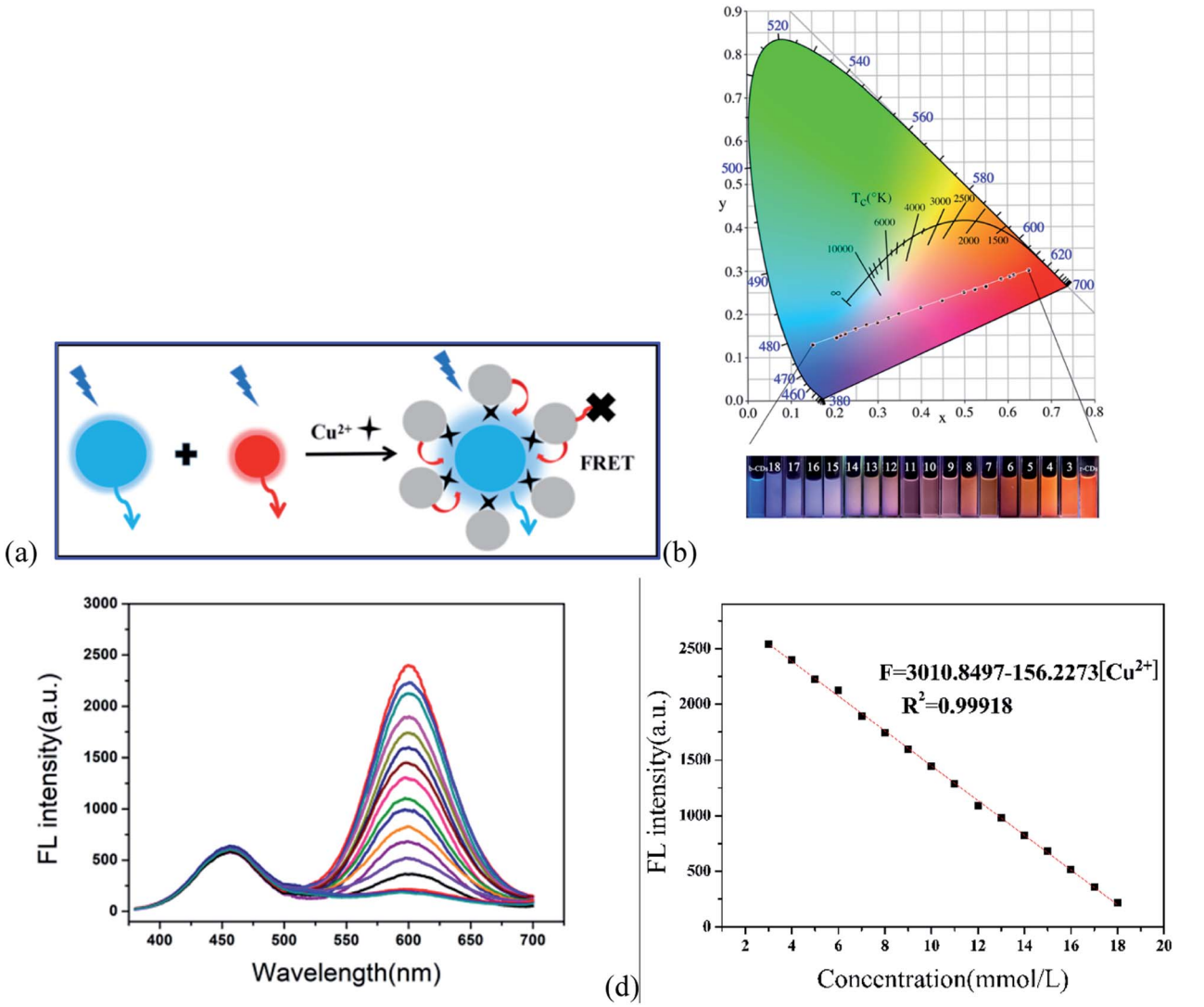

Fig. 6 (a) Interaction between r-CDs and Cu^{2+} ions by LMCT. (b) Chromaticity coordinates and digital images of the liquid phase ratio sensor under ultraviolet irradiation (numbers 3–18 represent Cu^{2+} concentrations of 3, 4, 5, 6, 7, 8, 9, 10, 11, 12, 13, 14, 16, 17 and 18 μmol L^{-1}, respectively). (c) Fluorescence spectra of r-CDs/b-CDs after adding different concentrations of Cu^{2+}. (d) Linear fitting curve of the fluorescence intensity at 600 nm (F) with Cu^{2+} concentrations of 3–18 μmol L^{-1}.

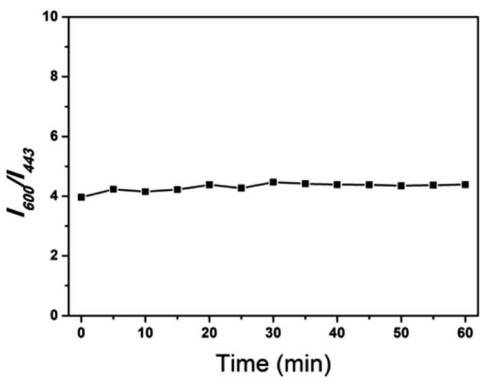

Fig. 7 Photostability of the ratiometric fluorescent I_{600}/I_{443} of mixing r-CDs/b-CDs with time of exposure to 360 nm ultraviolet light (I_{600} and I_{443} are the fluorescence intensities of r-CDs and b-CDs, respectively).

the paper by ink-printing, it was found that the detection color gamut of Cu^{2+} only changed from purple to blue, and the visualization effect was not obvious, as shown in Fig. 9. The content of r-CDs was thus increased.

Therefore, two-color carbon dots with different density values were inkjet printed on paper: the neutral r-CDs and b-CDs (pH 7.4) were used as red and blue fluorescent inks, respectively, for ink-jet printing on securities paper to prepare the fluorescent test paper. The fluorescence brightness of the test paper could be enhanced by repeated inkjet printing 10 times. As shown in Fig. 10a, the test paper with fluorescent ink was light pink under sunlight and showed a highly uniform orange-red fluorescence under the irradiation of a 365 nm UV lamp. The concentration of Cu^{2+} in the water was tested by directly observing the color of the test paper under an ultraviolet lamp.

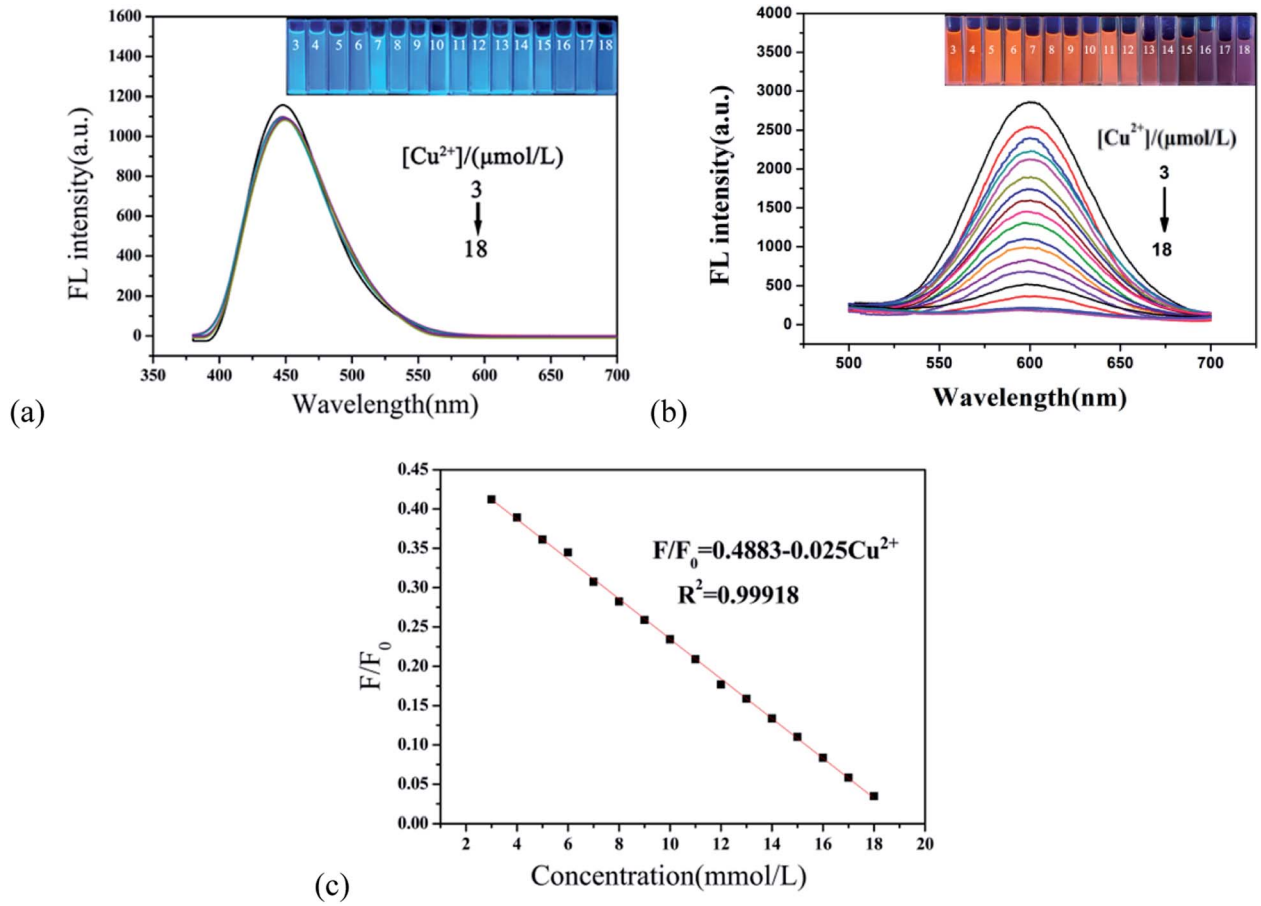

Fig. 8 (a) Fluorescence spectra of the b-CDs after adding different concentrations of Cu^{2+} (inset shows the blue fluorescence color change); (b) fluorescence spectra of the r-CDs after adding Cu^{2+} in a concentration range of 3 to 18 μmol L^{-1} (inset shows the orange-red fluorescence color change); (c) the linear fitting curve of the fluorescence intensity ratio (F/F_0) of the ratiometric probe *vs.* Cu^{2+} concentration.

The fluorescence response of the ratio paper-based sensor depended on the emission intensity at 443 and 600 nm, which was closely related to the density of r-CDs and b-CDs in the inkjet printing. As shown in Fig. 10b, when the density ratio of r-CDs/b-CDs was 10 : 1 or 10 : 2 (the content of r-CDs was high), the orange-red fluorescence of the detection paper was strong, which could completely shield the blue fluorescence. The Cu^{2+} concentration-related color change detected on the paper-based sensor was only close to purple. However, when the density ratio was 10 : 4 or 10 : 5 (the ratio of r-CDs became low), the red fluorescence was covered by the blue fluorescence of the b-CDs, and the Cu^{2+} concentration-related color change was not obvious. It can be seen that a too high or too low ratio of r-CDs/b-CDs may lead to very significant changes in the fluorescence color. In the ratio of 10 : 3, as shown in Fig. 10c, an obvious fluorescence color transition from orange to blue can be observed. Therefore, the r-CDs/b-CDs ratiometric probe with a pH of 7.4 and a density ratio of 10 : 3 was regarded as the best conditions in the following experiments. When the detection concentration range of Cu^{2+} was in the range of 3–18 μmol L^{-1}, there was a continuous evolution from orange-red to pink to purple to blue on the paper to realize visual detection. Fig. 10d can be used as a standard contrast color card to preliminarily determine the concentration range of Cu^{2+} detection by the naked eye.

Fig. 9 The range of color change reflected by Cu^{2+} with the same density value of r-CDs/b-CDs ink-jet printed on paper (compared with a reference color card).

3.4 Sensor selectivity and interference detection of Cu^{2+}

As shown in Fig. 11a, to research the selectivity of the r-CDs/b-CDs probe to Cu^{2+}, the fluorescence intensity ratios (F/F_0) under the same conditions with different metal ions were tested, including Ag^{+}, Co^{2+}, Ba^{2+}, Al^{3+}, Mn^{2+}, Fe^{2+}, K^{+}, Na^{+}, Zn^{2+}, Ni^{+}, and Cu^{2+}. It can be seen that the fluorescence intensity of the ratiometric fluorescence probe was quenched by about 77.97% at 600 nm after adding 10 μmol L^{-1} Cu^{2+}.

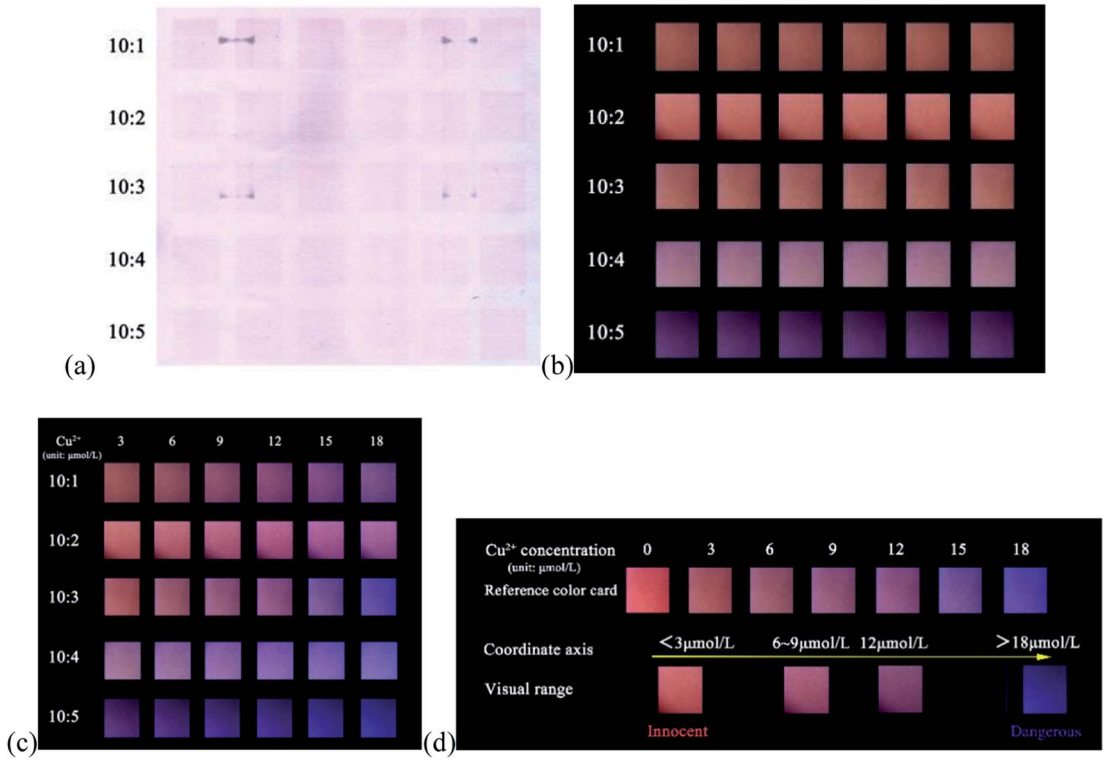

Fig. 10 (a) Paper-based sensors under natural light. (b) Fluorescence maps of paper-based sensors at 365 nm. (c) Fluorescence maps of Cu^{2+} in the concentrations of 3, 6, 9, 12, 15 and 18 μmol L^{-1} are printed successively on paper-based sensors (10 : 1–10 : 5 denotes the density ratio of r-CDs to b-CDs in ink-jet printing; 3–18 μmol L^{-1} denotes the ink-jet printing concentration of Cu^{2+}, with the density value of 100%). (d) Comparison of standard color cards for Cu^{2+} detection.

The fluorescence intensity did not decrease significantly with other ions. In contrast, the fluorescence intensity ratio (F/F_0) of the probe changed significantly after adding 10 μmol L^{-1} Cu^{2+}. Obviously, the ratio probe can still detect Cu^{2+} in the presence of all possible interference ions. The excellent selectivity and excellent anti-interference can be attributed to the higher affinity of Cu^{2+} to ρ-PDA-r-CDs/b-CDs than of the other metal ions (Fig. 11b).

The fluorescence changes of the paper-based sensor with the different metal ions were tested to study the specific response of the ratio-based paper-based sensor to Cu^{2+}. As shown in Fig. 12a, the fluorescence quenching effect of Cu^{2+} on the sensor was higher than that of other metal ions under the naked eye. To research the applicability of the test paper, the ten metal ion solutions were mixed with a certain concentration of Cu^{2+} solution. The fluorescent test paper showed obvious color responses to different Cu^{2+} concentrations (in Fig. 12a). It

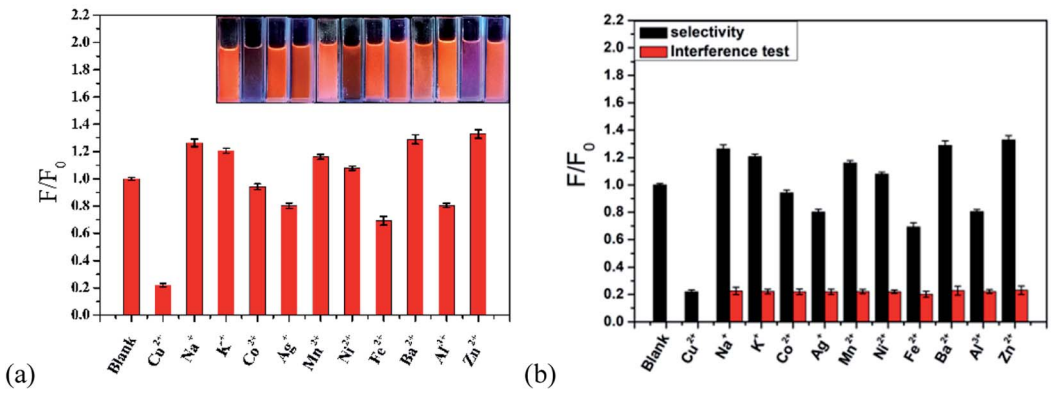

Fig. 11 (a) Fluorescence responses to 10 μmol L^{-1} different metal ions and Cu^{2+} ions in PBS buffer (pH 7.4) with the r-CDs b-CDs sensor (fluorescence intensity ratio 10 : 3). (b) The interferences are tested using a mixture of excess 10 μmol L^{-1} of interfering ions (black bars) with 10 μmol L^{-1} Cu^{2+} ion (red bars). The inset shows the corresponding fluorescence observed under a 365 nm UV lamp.

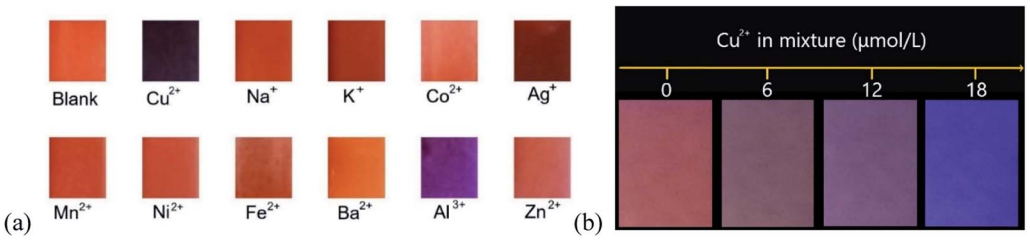

Fig. 12 Anti-interference visual detection of the ratio fluorescent test paper for (a) single metal ions and (b) a mixed solution.

turned blue completely when the concentration was 18 μmol L^{-1}. The results showed that our fluorescent test paper could meet the requirements of semi-quantitative detection of Cu^{2+} under the interference of other ions. It also shows the good selectivity of the paper-based sensor for Cu^{2+} detection and the possibility of the sensor to detect Cu^{2+} in practical applications.

4. Conclusion

First, CA and EDA were used to prepare b-CDs. They were dispersed in ethanol with a higher PLQY. A dual-color fluorescence ratio ratiometric test paper was made with r-CDs/b-CDs. B-CDs and r-CDs were used in inkjet printing at a density ratio of 3 : 10 to realize the fluorescence visualization detection of Cu^{2+}. The orange-red fluorescence of the r-CDs at 600 nm could be quenched because of the competitive binding between ρ-PDA on the surface of the r-CDs and Cu^{2+} in solution. Because the blue fluorescence of b-CDs at 443 nm was almost unaffected, a continuous broad-color evolution from orange to blue can be observed when Cu^{2+} with an increased concentration was added under a 365 nm UV lamp. Single r-CDs and r-CDs/b-CDs were used to compare the results, and the intensity reduction of the single CDs was so insignificant that the naked eye could not distinguish it well, especially for a low concentration of Cu^{2+}. Therefore, the dual-emission fluorescence paper-based sensor would be a good choice for Cu^{2+} vision detection. The ink-jet printing paper prepared with dual-colored CDs ink showed a dose-sensitive color response with a distinguishable scale as low as 3 μmol L^{-1} Cu^{2+}, which could be observed by the naked eye. The sensor has a large change in fluorescence color difference in the range of 3–18 μmol L^{-1} Cu^{2+}, which fully shows the possibility of semi-quantitative detection of Cu^{2+} by the paper-based sensor. Moreover, the filter paper was replaced with non-fluorescent bond paper, which increased the accuracy of the test paper. In addition, CDs are environmentally friendly compared to other tested substances and can be tested without recycling in the natural environment. The results of the paper suggest the unique optical properties of nanomaterials to develop promising visual test papers for environmental and medical applications.

Data availability

The data used to support the findings of this study are included within the article.

Conflicts of interest

The authors declare that there is no conflict of interest regarding the publication of this paper.

Acknowledgements

The authors gratefully recognize the financial support from the Key Laboratory of Intelligent and Green Flexographic printing (ZBKT202002; ZBKT201903).

References

1 Y. J. Zhou, X. Y. Huang, C. Liu, *et al.*, Color-Multiplexing-Based Fluorescent Test Paper: Dosage-Sensitive Visualization of Arsenic (III) with Discernable Scale as Low as 5 ppb, *Anal. Chem.*, 2016, **88**, 6105–6109.
2 C. Yuan, B. H. Liu, F. Liu, *et al.*, Fluorescence "Turn On" Detection of Mercuric Ion Based on Bis(dithiocarbamato) copper (II) Complex Functionalized Carbon Nanodots, *Anal. Chem.*, 2014, **86**, 1123–1130.
3 Y. H. Wang, C. Zhang, X. C. Chen, *et al.*, Ratiometric fluorescent paper sensor utilizing hybrid carbon dots-quantum dots for the visual determination of copper ions, *Nanoscale*, 2016, **8**, 5977–5984.
4 X. Y. Huang, Y. J. Zhou, C. Liu, *et al.*, A single dual-emissive nanofluorophore test paper for highly sensitive colorimetry-based quantification of blood glucose, *Biosens. Bioelectron.*, 2016, **86**, 530–535.
5 C. L. Jiang, B. H. Liu, M. Y. Han, Z. P. Zhang, *et al.*, Fluorescent Nanomaterials for Color-Multiplexing Test Papers toward Qualitative/Quantitative Assays, *Small Methods*, 2019, **2**, 1700379.
6 X. Liu, N. Zhang, T. Bing, *et al.*, Carbon Dots Based Dual-Emission Silica Nanoparticles as a Ratiometric Nanosensor for Cu^{2+}, *Anal. Chem.*, 2014, **85**, 2289–2296.
7 C. Liu, D. Ning, C. Zhang, *et al.*, Dual-colored carbon dot ratiometric fluorescent test paper based on a specific spectral energy transfer for semiquantitative assay of copper ions, *ACS Appl. Mater. Interfaces*, 2017, **22**, 18897–18903.
8 H. J. Plaehn, Y. L. Gu, K. Kaker, L. Gearheart, R. Ray, *et al.*, Electrophoretic analysis and purification of fluorescent single-walled carbon nanotube fragments, *J. Am. Chem. Soc.*, 2004, **40**, 12736–12737.

9 E. B. Secor and M. C. Hersam, Emerging Carbon and Post-Carbon Nanomaterial Inks for Printed Electronics, *J. Phys. Chem. Lett.*, 2015, **4**, 620–626.

10 J. Li, F. Rossignol and J. Macdonald, Inkjet printing for biosensor fabrication: combining chemistry and technology for advanced manufacturing, *Lab Chip*, 2015, **12**, 2538–2558.

11 A. L. Rutz, K. E. Hyland, A. E. Jakus, *et al.*, A Multimaterial Bioink Method for 3D Printing Tunable, Cell-Compatible Hydrogels, *Adv. Mater.*, 2015, **27**, 1607–1614.

12 J. P. Lombardi, R. S. Aga, E. M. Heckman, *et al.*, Characterization of DNA biopolymer-based UV photodetector fabricated by inkjet printing, *Electron. Lett.*, 2015, **51**, 778–780.

13 K. Jiang, S. Sun, L. Zhang, Y. Lu, A. G. Wu, C. Z. Cai and He. W. Lin, Red, Green, and Blue Luminescence by Carbon Dots: Full-Color Emission Tuning and Multicolor Cellular Imaging, *Angew. Chem., Int. Ed.*, 2015, **54**, 5360–5363.

14 H. Ding, S. B. Yu, J. S. Wei, *et al.*, Full-Color Light-Emitting Carbon Dots with a Surface-State-Controlled Luminescence Mechanism, *ACS Nano*, 2015, **10**, 484–491.

15 C. Zheng, X. Q. An and J. Gong, Novel pH sensitive N-doped carbon dots with both long fluorescence lifetime and high quantum yield, *RSC Adv.*, 2015, **5**, 32319–32322.

16 W. H. Zhou. *Research on the coating characteristics and printing performance of inkjet printing paper based on optical recognition*. South China University of Technology, 2014.

17 D. Qu. *Preparation and application of doped graphene quantum dots*. Changchun Institute of Optics, Fine Mechanics and Physics, Chinese Academy of Sciences. 2017.

18 Jaidev and S. Ramaprabhu, Poly(p-phenylenediamine)/graphene nanocomposites for supercapacitor applications, *J. Mater. Chem.*, 2012, **22**, 18775.

19 Y. L. Min, T. Wang, Y. G. Zhang, *et al.*, The synthesis of poly(p-phenylenediamine) microstructures without oxidant and their effective adsorption of lead ions, *J. Mater. Chem.*, 2011, **21**, 6683–6690.

20 A. Karimzadeh, M. Hasanzadeh, N. Shadjou, *et al.*, Electrochemical biosensing using b-CDs: Recent advances in analytical approach, *TrAC, Trends Anal. Chem.*, 2018, **105**, 484–491.

21 J. Soleymani, M. Hasanzadeh, M. H. Somi, *et al.*, Targeting and sensing of some cancer cells using folate bioreceptor functionalized nitrogen-doped graphene quantum dots, *Int. J. Biol. Macromol.*, 2018, **118**, 1021–2034.

22 Z. Y. Li, T. Bian, *et al.*, Highly luminescent nitrogen-doped carbon quantum dots as effective fluorescent probes for mercuric and iodide ions, *J. Mater. Chem. C*, 2015, **3**, 1922–1928.

23 J. M. Liu, L. P. Lin, X. X. Wang, *et al.*, Highly Selective and Sensitive Detection of Cu^{2+} with Lysine Enhancing Bovine Serum Albumin Modified-Carbon Dots Fluorescent Probe, *Analyst*, 2012, **137**, 2637–2642.

24 Y. Dong, R. Wang, G. Li, *et al.*, Polyamine-Functionalized Carbon Quantum Dots as Fluorescent Probes for Selective and Sensitive Detection of Copper Ions, *Anal. Chem.*, 2012, **84**, 6220–6224.

25 C. M. Jones, C. R. Johnson, S. A. Asher, *et al.*, Resonance Raman Studies of the Excited Electronic States of $(CN)_5$FeIII(imidazole)$_2$– and $(NH_3)_5$RuIII(imidazole)$^{3+}$, *J. Am. Chem. Soc.*, 1985, **107**, 3772–3780.

26 E. Bernarducci, P. K. Bharadwaj, K. Krogh-Jespersen, *et al.*, Electronic Structure of Alkylated Imidazoles and Electronic Spectra of Tetrakis(imidazole)copper (II) Complexes, *J. Am. Chem. Soc.*, 1983, **105**, 3860–3866.

27 E. Bernarducci, W. F. Schwindinger, J. L. Hughey, *et al.*, Electronic Spectra of Copper (II)-Imidazole and Copper (II)-Pyrazole Chromophores, *J. Am. Chem. Soc.*, 1981, **103**, 1686–1691.

28 K. Krogh-Jesperse and H. J. Schugar, Detailed Correlations between the Ligand-to-Metal Charge-Transfer (LMCT) Spectra of Copper (II) and Ruthenium (III) Imidazoles and Imidazolates. Electronic Structures of Carbon-Bound Ruthenium (III) Imidazoles and Imidazolates, *Inorg. Chem.*, 1984, **23**, 4390–4393.

29 T. G. Fawcett, E. Bernarducci and K. Krogh-Jespersen, Charge-Transfer Absorptions of Cu (II)-Imidazole and Cu (II)-Imidazolate Chromophores, *J. Am. Chem. Soc.*, 1980, **102**, 2598–2604.

30 L. Zhang, H. Wang, W. Yu, *et al.*, Facile and large-scale synthesis of functional poly(m-phenylenediamine) nanoparticles by Cu^{2+}-assisted method with superior ability for dye adsorption, *J. Mater. Chem.*, 2012, **22**, 18244–18251.

31 Y. Dong, H. Pang, H. B. Yang, *et al.*, Carbon-Based Dots Co-doped with Nitrogen and Sulfur for High Quantum Yield and Excitation-Independent Emission, *Angew. Chem., Int. Ed.*, 2013, **52**, 7800–7804.

32 Y. Song, S. Zhu, S. Xiang, *et al.*, Investigation into the fluorescence quenching behaviors and applications of carbon dots, *Nanoscale*, 2014, **6**, 4676.

33 R. Ye, C. Xiang, J. Lin, *et al.*, Coal as an abundant source of graphene quantum dots, *Nat. Commun.*, 2013, **4**, 2943.

34 Q. Mei, H. Jing, Y. Li, *et al.*, Smartphone based visual and quantitative assays on upconversional paper sensor, *Biosens. Bioelectron.*, 2016, **75**, 427.

35 H. Ding, S. B. Yu, J. S. Wei, *et al.*, Full-Color Light-Emitting Carbon Dots with a Surface-State-Controlled Luminescence Mechanism, *ACS Nano*, 2016, **10**, 484.